# Three-Dimensional FENE-CR Flow in a Cross-slot

*G.N. Rocha[1], R.J. Poole[2], M.A. Alves[3], P.J. Oliveira[1]*

*[1] Dpto. de Engenharia Electromecânica. Universidade da Beira Interior (Portugal).*
*[2] Dpt. of Engineering. University of Liverpool (United Kingdom).*
*[3] Dpto. de Eng. Química. CEFT. Faculdade de Engenharia da Universidade do Porto (Portugal).*

## Introduction

Many flows of practical relevance tend to develop elastic instabilities that are often a limitation in processing operations. Nowadays, considerable effort is expended in developing microfluidic devices which involve the flow of non-Newtonian fluids, and geometries with intersection of ducts are common (i.e. "cross-slot" flows). A numerical investigation of fully-developed flows of viscoelastic fluids through a 3D planar cross-slot is presented in this study. Our motivation here is to investigate 3D flow behaviour in which after the first instability the flow becomes deformed and asymmetric, but remains steady. A second instability occurs at higher strain rates and leads to a velocity field fluctuating non-periodically in time. Our 3D results reveal that, as occurred for the 2D cases, asymmetric flows do arise under perfectly symmetric flow conditions. The results are consistent with the recent experimental study of Arratia et al. [1] and the 2D simulations of Poole et al. [2]. Detailed simulations are conducted for varying aspect ratio ($AR$) of the 3D geometry encompassing both square and rectangular cross-sections.

## Governing Equations and Numerical Method

The basic equations for the three-dimensional (3D), incompressible and isothermal, laminar fluid flow problem to be solved are those expressing conservation of mass and linear momentum:

$$\frac{\partial u_i}{\partial x_i} = 0 \tag{1}$$

$$\frac{\partial \rho u_i}{\partial t} + \frac{\partial \rho u_i u_j}{\partial x_j} = -\frac{\partial p}{\partial x_i} + \frac{\partial \tau_{ij}}{\partial x_j} \tag{2}$$

where $\rho$ is the fluid density (assumed constant) and $u_i$ the velocity component along the Cartesian directions $x_i$. Einstein's summation for repeating indices is assumed in all equations. The dependent variables are the velocity components, pressure $p$ and the extra stress components $\tau_{ij}$, which need to be specified by means of a rheological constitutive equation. In this work two types of constitutive equations are considered. The first is the Newtonian model,

$$\tau_{ij} = \eta_s \left( \frac{\partial u_i}{\partial x_j} + \frac{\partial u_j}{\partial x_i} \right) \tag{3}$$

where $\eta_s$ is the solvent viscosity. As a second type of constitutive equation adequate for modelling viscoelastic flow behaviour, the FENE-CR model [3] is adopted, which is expressed by the following differential transport-like equation for $\tau_{ij}$:

$$\tau_{ij} + \lambda \left( \frac{1}{f} \left[ \left( \frac{\partial \tau_{ij}}{\partial t} + u_k \frac{\partial \tau_{ij}}{\partial x_k} \right) - \tau_{ik} \frac{\partial u_j}{\partial x_k} - \tau_{jk} \frac{\partial u_i}{\partial x_k} \right] + \tau_{ij} \left( \frac{\partial (1/f)}{\partial t} + u_k \frac{\partial (1/f)}{\partial x_k} \right) \right) = \eta_p \left( \frac{\partial u_i}{\partial x_j} + \frac{\partial u_j}{\partial x_i} \right) \tag{4}$$

The function $f$ is expressed by:

$$f = \frac{L^2 + \left(\lambda/\eta_p\right)\tau_{kk}}{L^2 - 3} \qquad (5)$$

where $\lambda$ is the constant zero-shear rate relaxation time, $\eta_p$ the contribution of the polymer to the total shear viscosity $\eta_0 = \eta_s + \eta_p$ (also taken as constant) and $L^2$ the extensibility parameter that measures the elongational viscosity. The relevant dimensionless parameters are: $L^2$, the extensibility parameter of the FENE-CR model; $\beta = \eta_s/\eta_0$, the solvent viscosity ratio; $Re = \rho U d/\eta_0$, the Reynolds number (neglected in this study, i.e. creeping flow is assumed); and $De = \lambda U/d$, the Deborah number. A fully implicit finite-volume method is used to solve the previous equations which have been described in great detail in previous works [see e.g. 4]. Boundary conditions are required for the dependent variables at the boundary faces of computational domain and we impose fully-developed velocity (average velocity $U$) and stress profiles at inlet, Neumann boundary conditions at the outlets and no-slip conditions at the walls.

## Flow Geometry and Computational Mesh

The cross-slot geometry is shown in Fig. 1, where details of the relevant parameters are provided. Flow enters from the left and right "arms" and leaves from top and bottom channels, with widths $d$ and lengths 10$d$. The top and bottom channels are sufficiently long for the outlet flow to become fully-developed; thus avoiding any outlet condition effect upon the flow in the central region of the cross-slot, which is the main focus of attention here. The aspect ratio of the cross-slot is connected to 3D effects and is here defined as $AR = H/d$, where $H$ represents the depth of the geometry, which was varied between three values of $AR$ = 1 (cubic cross-section), 2 and 4.

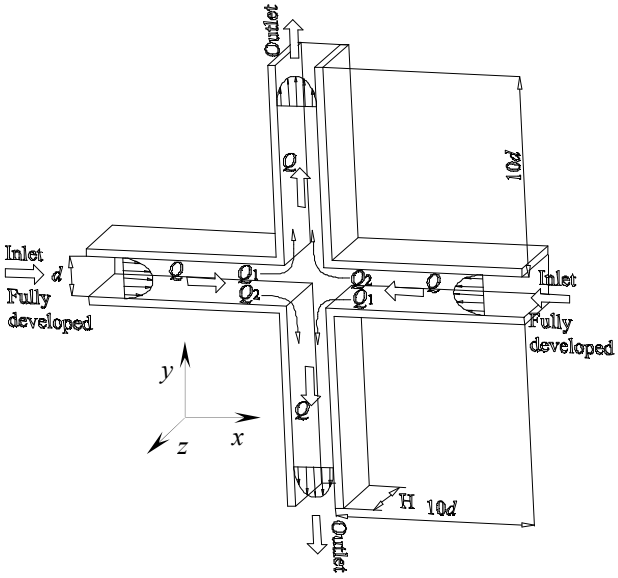


*Figure 1. Schematic of cross-slot 3D geometry.*

The mesh used in the numerical simulations is composed of 78125 cells which results in 781250 degrees-of-freedom. A similar mesh was employed in [5] where a related study with the UCM model was reported.

## Results and Discussion

In order to quantify the degree of flow asymmetry we employ the same non-dimensional flow-rate imbalance parameter, $DQ = \left(Q_1 - Q_2\right)/Q$ defined by Poole et al. [2], where the flow rates $Q_1$ and $Q_2$ are indicated in Fig.1. The total flow rate in each incoming channel is $Q = Ud$ and it is subsequently divided at the cross-slot region into two equal or unequal flow rates such that $Q = Q_1 + Q_2$. For a symmetric flow $Q_1 = Q_2$ and $DQ = 0$, while for an asymmetric flow $Q_1 \neq Q_2$ and $DQ \neq 0$ (completely asymmetric flow $DQ = \pm 1$). In Fig. 2 we compare the streamline patterns at the cross-slot center plane ($z$ = 0) for increasing values of Deborah number, and fixed $L^2$ = 100 and $\beta = 0.1$, with variation of the aspect ratio ($AR$).

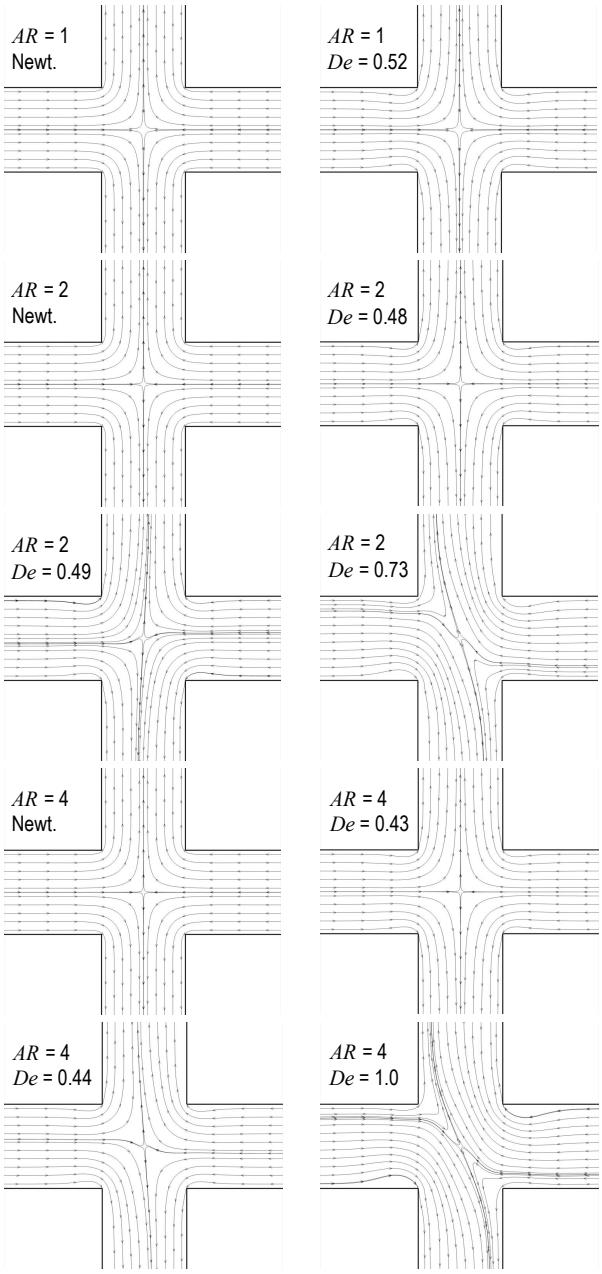


*Figure 2. Predicted streamline plots at the center plane.*

As a limiting case we have $AR \rightarrow \infty$ which corresponds to a two-dimensional (2D) flow already investigated in a previous work [6]. In such a limiting 2D geometry the flow becomes increasingly asymmetric but remains steady for Deborah number above a critical value, which is $De_{\mathrm{cr}} \approx 0.46$, for the parameters $L^2 = 100$ and $\beta = 0.1$ here employed until Deborah number of 1.0 is reached, when unsteadiness sets in. With the 3D geometry for $AR = 1$ the flow patterns remains perfectly symmetric without signs of bifurcation, until the onset of an elastic instability that leads to the flow becoming periodic for $De \geq 0.52$. At the two values of aspect ratio $AR = 2$ and 4 we found the existence of two flow instabilities:

- Steady asymmetric flow:
  - $AR = 2 \rightarrow De_{\mathrm{cr}} \approx 0.49$;
  - $AR = 4 \rightarrow De_{\mathrm{cr}} \approx 0.44$.
- Periodic flow (time-dependent instability):
  - $AR = 2 \rightarrow De \geq 0.73$;
  - $AR = 4 \rightarrow De \geq 1.0$.

The situation is exemplified in Fig. 2: with the aspect ratio of $AR = 2$, the results start from $De = 0$ (Newtonian – symmetric flow), 0.48 (just before bifurcation), 0.49 (just after bifurcation) and 0.73 (just after periodic flow). It is clear that in this geometry the asymmetry of the flow is triggered by elasticity, since the simulations are for creeping flow ($Re = 0$), and the point of $De_{\mathrm{cr}}$ defines the first transition point from a symmetric to an asymmetric state. In addition, the results in Fig. 2 show that an increase in the aspect ratio ($AR$) tends to accentuate the steady bifurcation phenomenon, that is, the end walls bring a stabilising influence to this flow which increases as the distance between those walls gets smaller. On the other hand, the unsteady instability occurs at progressively lower $De$ values as the $AR$ of the cross-slot decreases. The 3D nature of the flow is exemplified in Fig. 3 which presents projected streamline patterns in planes close to the walls at $|z/H| \rightarrow 1/2$ ($AR = 1$), 1 ($AR = 2$) and 2 ($AR = 4$), for the same cases of Fig. 2. By contrasting these two figures it is possible to have an impression of the 3D effects that go on along the depth of the cross-slot.

Due to the 3D nature of the flow all cases which exhibit the bifurcation phenomenon present a more accentuated asymmetry in the streamline plots at the center plane ($z = 0$), while near the walls the streamline flow patterns appear much more symmetric. We can thus conclude from Fig. 3 that the cross-slot end walls tend to stabilize the asymmetric flow for aspect ratios

$AR$ = 2 and 4, and that for $AR$ = 1 the asymmetric flow does not even appear. Instead, the only evidence is of periodic instability, as previously discussed.

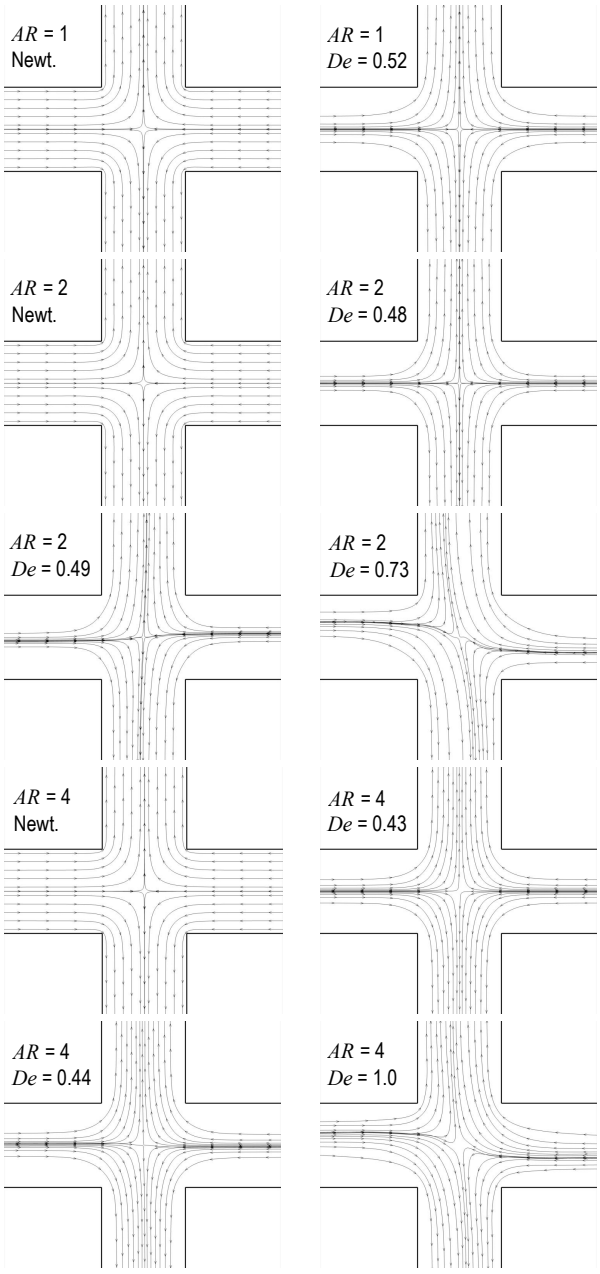


*Figure 3. Predicted streamline plots near the walls.*

## Concluding Remarks

3D effects have important implications on the onset of either steady or unsteady flow bifurcations in cross-slot geometries. The effect of the end walls, which is enhanced by decreasing the aspect ratio, tends to stabilise the first steady, critical transition point. With $AR$ = 1, no bifurcation to asymmetric flow is observed. On the other hand, the critical unsteady-flow transition is observed at lower $De$ when $AR$ is reduced. Therefore, 3D flow are more prone to go through a symmetric-steady to unsteady transition rather than symmetric to asymmetric-steady transitions as in 2D flows.


## Acknowledgements

The authors would like to acknowledge the financial support from FCT (Portugal) under projects PTDC/EME-MFE/70186/2006, PTDC/ EQU-FTT/71800/2006 and the Ph.D. scholarship SFRH/BD/22644/2005 (G.N. Rocha).


## References


1. Arratia, P.E., Thomas, C.C., Diorio, J.D., and Gollub, J.P. (2006). Phys. Rev. Lett. 96, 144502.
2. Poole, R.J., Alves, M.A., and Oliveira, P.J. (2007). Phys. Rev. Lett. 99, 164503.
3. Chilcott, M.D., and Rallison, J.M. (1988). J. Non-Newtonian Fluid Mech. 29, 381–432.
4. Oliveira, P.J., Pinho, F.T., and Pinto, G.A. (1998). J. Non-Newtonian Fluid Mech. 79, 381–432.
5. Poole, R.J., Alves, M.A., Afonso, A.P., Pinho, F.T., and Oliveira, P.J. (2007). In AIChE Annual Meeting, Salt Lake City, USA.
6. Rocha, G.N., Poole, R.J., Alves, M.A., and Oliveira, P.J. (2008). In II CNMNMFT (Costa, V.A.F. et al., eds.), Universidade de Aveiro, Portugal.



*Contact Address:*

*Paulo Jorge dos Santos Pimentel de Oliveira (pjpo@ubi.pt)*
*Dpto. Engenharia Electromecânica*
*Universidade da Beira Interior, Calçada Fonte do Lameiro, Edifício das Engenharias, 6201-001 Covilhã (Portugal)*
*Telf.:+351 275329946; Fax:+351 275329972*